Iranian Polymer Journal (2020) 29:1087–1097
https://doi.org/10.1007/s13726-020-00863-z

ORIGINAL RESEARCH

Characterization of carboxymethyl cellulose-based active films incorporating non-modified and Ag or Cu-modified Cloisite 30B and montmorillonite nanoclays

Seyed Jamaleddin Peighambardoust[1] · Sirous Zahed-Karkaj[2] · Seyed Hadi Peighambardoust[3] · Yadollah Ebrahimi[1] · Donatella Peressini[4]

Received: 5 May 2020 / Accepted: 5 September 2020 / Published online: 13 September 2020

Abstract

Physico-mechanical and antibacterial properties of carboxymethyl cellulose (CMC)-based films incorporating Cloisite 30B (C30B) and montmorillonite (MMT) clay nanoparticles (NPs) modified with Ag and Cu ions were investigated. X-Ray diffraction patterns for modified clays with Ag and Cu ions showed that they were effectively located in the interlayer space of C30B and MMT clay NPs and increased their interlayer spacing. Scanning electron microscopy showed a smooth and homogeneous structure for a pure CMC film. Films containing MMT had coarser and more heterogeneous surface compared to C30B film, suggesting a better dispersion of modified C30B in the matrix of CMC. Mechanical analysis showed that films containing Ag- or Cu-modified C30B NPs exhibited higher tensile strength than that of MMT films. The ultraviolet spectroscopy showed that nanocomposite films containing Ag modified C30B had the highest UV absorption compared to other samples. Water vapor permeability of CMC films loaded by Ag- or Cu-modified C30B and MMT NPs significantly decreased compared to those of non-modified types and control. Microbial tests revealed that Ag-modified clay NPs had significantly higher antibacterial activity than Cu-modified types against *E. coli* and *S. aureus* bacteria. Films loaded with non-modified C30B NPs had the second most antibacterial effect followed by non-modified MMT NPs and control films.

Keywords Antimicrobial · Clay · CMC · Mechanical · Packaging · Physical · Nanocomposite films

Introduction

There is a global interest in the development of novel, green and cost-effective packages that preserve food products quality [1]. Most packaging materials are based on non-degradable plastic polymers causing copious amounts of waste resulting in environmental pollution [2]. Studies have shown that more than half of the waste in the industrialized countries is produced by packaging materials [3].

It is well known that the biodegradability of petroleum-based plastic materials is a very slow process due to their non-polar nature causing a serious environmental problem called white contamination. Thus, substitution of plastic packaging films with biodegradable material sources and natural macromolecules would reduce the environmental pollution and preserve fossil fuel resources [4]. Unlike synthetic plastic materials, biodegradable polymers are converted into natural products such as carbon dioxide, water, methane, and biomass during the composting process [5]. Carbohydrate polymers such as cellulose, starch, and their derivatives are potential renewable and cheap sources of sustainable packaging materials possessing a high degree of biodegradability. Carboxymethyl cellulose (CMC) is a biodegradable and non-toxic compound, which is used in many applications such as coating, food packaging, drug

✉ Seyed Jamaleddin Peighambardoust
j.peighambardoust@tabrizu.ac.ir

✉ Seyed Hadi Peighambardoust
peighambardoust@tabrizu.ac.ir

[1] Faculty of Chemical and Petroleum Engineering, University of Tabriz, Tabriz, Iran

[2] Faculty of Engineering, Islamic Azad University, Ahar Branch, Ahar, Iran

[3] Department of Food Science, College of Agriculture, University of Tabriz, Tabriz, Iran

[4] Department of Agricultural, Food, Environmental and Animal Sciences, University of Udine, 33100 Udine, Italy

delivery systems, textile printing and paper industry [6]. Nevertheless, CMC films show poor mechanical and water vapor barrier characteristics at high relative humidity conditions, leading to a restriction of their potential usage for packaging films [7]. Resistance of a film against moisture permeation is a key feature of biocomposite films in applications where food inside the package must be protected against humid atmosphere.

Incorporation of reinforcing nano-fillers into CMC polymer matrix enhances barrier potential and reinforces physical and mechanical strength of the resulting film [8]. For this reason, nano-fillers are used to increase the mechanical strength and enhance the barrier properties of biodegradable films [9, 10]. The importance of using nanoparticles (NPs) as fillers is due to their role in increasing the compatibility between mixed components [11] due to their nanosize and large surface/volume ratio and activity [12]. Besides, nano-fillers are considered as carrier of active ingredients, such as antimicrobials and antioxidants to preserve microbiological quality of packaged food products [13, 14]. There are many studies reporting on improved characteristics of different bio-nanocomposite films loaded with nano-fillers [15–17].

In a previous study, properties of CMC-based films incorporating Ag, ZnO and CuO NPs added as individual versus combinatorial mode were investigated [18, 19]. Results showed that using a combination of metallic NPs in CMC matrix revealed a synergism in improving antibacterial and physical strength of bio-nanocomposite films [20, 21]. This would help in development of antimicrobial films with reduced amounts of nanometal fillers. The incorporation of inorganic NPs, such as nanoclay and montmorillonite (MMT) into bio-nanocomposites results in their improved mechanical strength and permeability against water vapor, O_2, CO_2 and other volatile compounds [22, 23]. MMT is a highly hydrophilic clay that has good absorption capability, high transfer capacity, and the ability to be a carrier of materials [14]. Clays, zeolites, and other alumino-silicates have been used in food packaging because they have high ion-exchange capacity, surface area, and absorption capacity, active surface, chemical inactivity, and low or no toxicity. MMT attacks and absorbs negative charge bacteria after being released into the water and increases antimicrobial properties of the material. It is also a good absorbent for organic molecules such as aflatoxins, salicylic acid, herbicides and fungicides [24].

Antimicrobial minerals are generally based on metal ions with antimicrobial properties such as Ag^+ and Cu^{2+}, which are loaded in the matrix by ion-exchange mechanism. Surface modification of these NPs with metal ions including Cu, Ag, Zn, Pd, and Ti provides antibacterial effects to these ions [25, 26]. Antimicrobial activity of these metallic ions against a very broad spectrum of bacteria, yeasts, and fungi has been reported while they have no negative effect on eukaryotic cells [27, 28]. However, the concentration of metallic ions such as Ag in food packaging materials should be kept at minimum due to their potential toxicity and possible migration from packaging material into food [13, 29]. It is documented that nanoclays with active or functionalized surface can have enhanced antibacterial activity, improved NPs physical stability and dispersion [30]. Besides, surface activation of clay NPs with metallic ions could decrease their required minimum dose for antimicrobial effects, hence making these NPs less toxic [31].

In a recent study, we reported on the antibacterial properties' films based on corn starch which incorporated with different concentrations of Ag- or Cu-modified clay NPs. We showed that clay NPs with activated surface enhanced the antibacterial properties of resulting starch-based films [32]. In the current study, CMC-based nanocomposites were used as biopolymer matrix and the aim of the work was to modify C30B and MMT clay NPs with silver and copper ions and investigate the physical, mechanical, and antibacterial properties of CMC-based films containing the modified clay NPs.

Experimental

Materials

CMC (molecular weight 41,000g mol^{-1}) was obtained from Nippon Paper Group (Japan). Sodium montmorillonite (Na^+-MMT), an unmodified clay NPs was purchased from Sigma-Aldrich (France). Cloisite 30B (density: 1.98 g. mL^{-1}, interlayer space: 18.5 Å, moisture < 2%) was supplied by Southern Clay Products, Inc. (USA). Glycerol was obtained from Dr. Mojallali Co. (Tehran, Iran). *Escherichia coli* (ATCC 1330) and *Staphylococcus aureus* (ATCC 1189) were obtained from the Persian Type Culture Collection (PTCC, Tehran, Iran). Manitol salt agar (MSA) and sodium chloride were purchased from Marmadia Co. (Iran) and violet red bile agar (VRBA) was provided by Charles Co. (Italy).

Nanoclays surface modification with Cu and Ag ions

To obtain copper exchanged clay NPs of C30B and MMT, 5 g of each clay NPs was distributed in 250 mL of 0.1 mol L^{-1} $CuSO_4$. The dispersion was held at 60 °C for 6 h while gently stirring, followed by a centrifugation and filtering the sediment through 1.0 mm filters. The remaining sediment was washed and pH was adjusted to 5.6 followed by drying in an oven at 80 °C. The dried samples (C30B-Cu or MMT-Cu) were ground and sieved to obtain homogeneous powders. Ag exchanged clay NPs (C30B-Ag or MMT-Ag) were made using the same procedure, except that 0.02 mol L^{-1} $AgNO_3$ solution was used instead of $CuSO_4$

[32]. A schematic representation of the modification of clay NPs with metallic ions and preparing the composite films is shown in Fig. 1.

Preparation of CMC-based nanocomposite films containing clay NPs

Nanocomposite films were prepared by dissolving CMC in distilled water, casting of the biopolymer containing NPs solution and solvent evaporation by drying (Fig. 1). To make a homogenous distribution of NPs in CMC matrix, they were dispersed in 180 mL of distilled water and sonicated for 30 min in an ultrasonic bath. Then, 20 mL of distilled water together with 3 g of CMC was added to the solution. After complete dissolution of CMC, 1.5 mL glycerol was added to the solution and moderately stirred for 20 min. The solution was heated at 75 °C for 30 min in a water bath followed by cooling to room temperature. To remove any air bubbles in the solution, degassing was applied using a bath-type ultrasound device. Finally, the film-forming mixture was cast onto leveled glass plates and dried at 55 ± 2 °C, for 18 h to form the nanocomposite films. Film thickness was 120 ± 5 µm measured by a digital micrometer (Mitutoyo Manufacturing Co., Japan).

X-Ray diffraction (XRD)

Investigation on the structure of nanocomposite films was conducted using an X-ray diffractometer apparatus (D5000 Siemens, Germany) with a Cu-K_α radiation source at a wavelength of λ = 1.41 nm, voltage of 40 kV and current of 30 mA. The X-ray diffraction pattern of the samples was obtained in 2θ range from 1 to 10 degrees with a step size of 2° s^{-1} at a temperature of 25 °C. This analysis is used to calculate the distance between unmodified and modified clay sheets in nanocomposite films. There are two forms of NC sheets placing in polymer chains: (1) polymeric chains penetrate into the nanoclay interlayer space and NC layers maintain their natural structure and only intercalate (intercalated structure); (2) NC layers are completely separated and dispersed in different directions in the polymer matrix (exfoliated structures). After plotting the curves and determining the diffraction peak, the distance between the layers was calculated using the following Bragg's equation:

$$n\lambda = 2d\sin\theta, \tag{1}$$

where n is constant of the device ($n = 1$), λ is the wavelength of the incident beam ($\lambda = 0.1539$ nm), d is the basal spacing (named d001) between crystalline sheets (nm), and θ is X-ray reflection angle of the crystal sheet calculated from 2θ, which is the point on the curve in which the peak diffraction is observed.

Scanning electron microscopy (SEM)

SEM (LEO 1430VP; Carl Zeiss SMT, Oberkochen, Germany) was used to observe cross-section surface of CMC

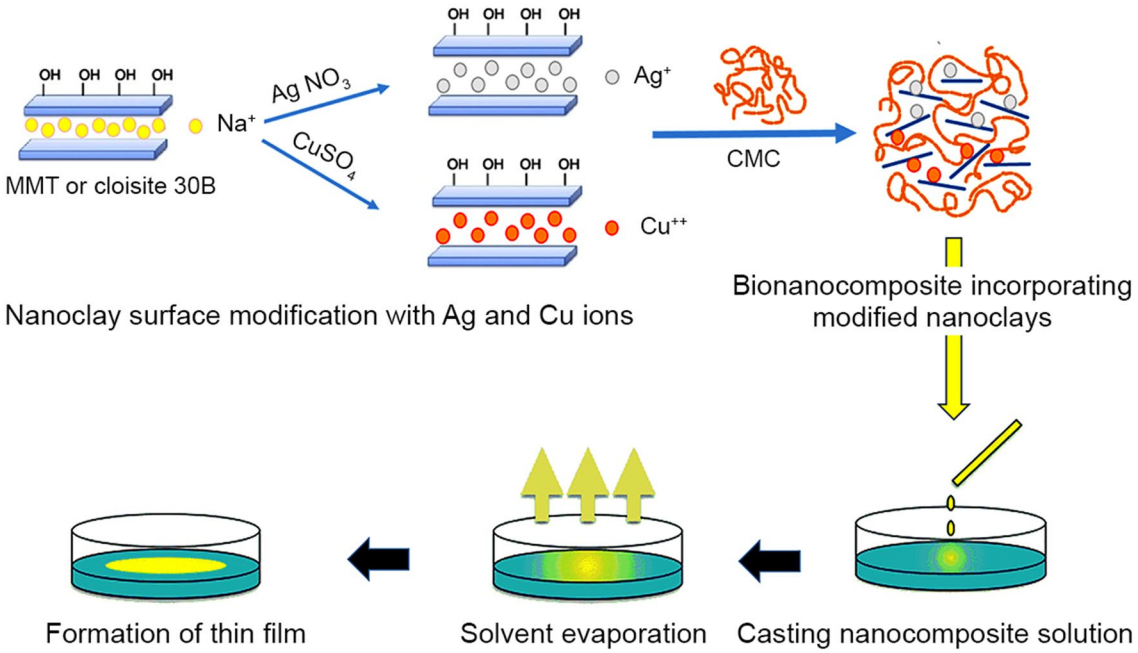

Fig. 1 A schematic representation of the modification of clay NPs with metallic ions and preparing the composite films

films. Dried film samples were frozen in liquid N_2 for 15 min and they were then broken to provide appropriate cross-sections followed by coating with a thin layer of gold (Au) for microscopic observation. A rising voltage of 1–15 kV was applied with a magnification of 20-fold [33].

Mechanical properties of film samples

Mechanical properties demonstrate the ability of films to preserve food against mechanical damage and deformation during handling [34]. Therefore, depending on the type of packaged material, the choice of packaging film with the desired mechanical properties will have particular importance in increasing the shelf life of the product [30]. Tensile strength (TS) and elongation-at-break (E) of films were measured by uniaxial tensile tests using a Zwick/Roell FR010 testing machine (Germany) according to ASTM D882-18 method. Film strips (60 × 20 mm) were kept at relative humidity (RH) of 53% for 48 h for conditioning before mechanical analysis. Samples were stretched at elongation speed of 5 mm $min^{-1}$and initial gauge of 40 mm at room temperature (25 °C) [35]. Mechanical tests were conducted in triplicate. TS (MPa) and E (%) were calculated using following equations:

$$\mathrm{TS} = \frac{F_{\max}}{A_{\min}}, \tag{2}$$

$$E = \frac{L_{\max}}{L_0} \times 100, \tag{3}$$

where F_{max} (N) is the maximum extensional force, A_{min} (m^2) is the minimum cross-sectional area, L_{max} (m) is amount of elongation at rupture, and L_0 (m) is the initial length of film sample.

UV–Visible spectroscopy

Film transparency relates to barrier properties against visible light and can be measured by a general spectrophotometer. Beer-Lambert's law (Eq. 4) describes a relationship between the attenuation of light through an object and the properties of that material.

$$A = \log\left(\frac{I_0}{I}\right) = \log\left(\frac{1}{T}\right), \tag{4}$$

where T is transmittance; A is absorbance; I_0 and I are the intensity of original light and of the light passed through the absorbing medium, respectively.

The UV–visible spectra were measured by a UV–vis double-beam spectrophotometer (Analytik Jena, Model SPECORD 250, Germany) according to ASTM D1746-15 method. The film strips (40 × 20 mm) were conditioned in a RH = 53% for 24 h. The optical absorbance of the film samples against air as reference was measured in the wavelength range of 200–800 nm. The transparency (% of transmitted light) of films was determined using the transmittance of light at 600 nm (T_{600}) from Eq. 5, which was derived from Eq. 4.

$$\text{Transparency} = \frac{(\log T_{600})}{L}, \tag{5}$$

where T_{600} indicates the transmittance at 600 nm and L is the thickness of the film (mm).

Water vapor permeability (WVP)

ASTM E96-16 method and Eq. 6 were applied to evaluate WVP (g m^{-1} h^{-1} Pa^{-1}) of films according to González Sandoval et al. [36] with few modifications. The test film discs ($\emptyset$ = 16 mm, 55% relative humidity, RH) were sealed to a glass vials ($\emptyset$ = 8 mm; H = 45 mm) containing anhydrous calcium sulfate (0% RH) and the vials were weighed and transferred into a desiccator maintained at 97% RH with a saturated salt solution of potassium sulfate and at 25 °C. The weight gain of the vials was measured periodically over a total time of 96 h, which indicated the amount of water vapor transferred from the films or water vapor transmission rate (WVTR). WVP was then calculated as follows:

$$\mathrm{WVP} = \frac{\mathrm{WVTR}}{\mathrm{A}} \frac{\mathrm{X}}{\Delta P_v}, \tag{6}$$

where WVTR is the water vapor transmission rate (g h^{-1}) which was calculated by plotting film weight gain data over time (h) through a linear regression ($R^2 > 0.98$) and the line slope was obtained as WVTR; X is the mean of film thickness (m); A is the area of WVT (m^2); and ΔP_v is the vapor pressure difference (3073.9 Pa) between the atmosphere of two sides of the films; inside the vial with anhydrous $CaSO_4$ with RH = 0% and the desiccator containing saturated KSO_4 solution with RH = 97%. In a specific term, WVTR was considered as the slope of curve plotting the final film weight (weight gain at the moment of measurement) minus the initial weight of the sample ($W_f - W_0$) over the time. Three replicates were conducted for the same treatment.

Antibacterial properties

Two types of bacteria *E. coli* (gram-negative) and *S. aureus* (gram-positive) were used for microbiological tests. The bacteria cells were first cultured in sterile culture media (30 g L^{-1} of de-ionized water) and incubated at 37 °C for 24 h. The desired initial values of 17.6×10^8 CFU mL^{-1} for *E. coli* and 18.6×10^8 CFU mL^{-1}

for *S. aureus* were considered. Antibacterial performance of pure CMC film as well as nanocomposite films containing clay NPs were evaluated by agar diffusion method (inhibition zone test) [1]. When antibacterial NPs were released from film discs located in the culture medium comprising the target microorganism, an inhibition zone around the film was formed. For the films with enhanced antibacterial effect the inhibition zone becomes larger in diameter. To evaluate the inhibitory range for appropriate culture media for each microorganism, MSA medium (111 g L^{-1} de-ionized water) was used for *S. aureus* and the VRBD medium (39.5 g L^{-1} de-ionized water) was used for *E. coli*. After preparation of the culture media in plates of 8 cm diameter, 1 mL of microorganism was poured onto the medium and spread by sterilized L-shaped rod. The prepared films discs ($d = 2$ cm) were placed in center of petri dishes containing culture media and then incubated at 37 °C for 24 h. The inhibition zone diameter (mm) was measured using a Vernier caliper in triplicates.

Statistical analysis

Statistical analysis was carried out using Minitab 16 software package. Significant differences among means were measured by one-way analysis of variance (ANOVA) and Tukey's test ($P < 0.05$).

Results and discussion

X-Ray diffraction analysis (XRD)

As mentioned in the experimental section, XRD analysis was used to study the structure of nanocomposite films. Crystalline XRD patterns of unmodified as well as Ag- and Cu-modified C30B NPs are shown in Fig. 2a. According to this pattern and calculated clay layers distances by Bragg's law, it was clear that the introduction of Ag and Cu ions increased the intercalations between C30B layers. Metal ions of Ag have been effectively located in the interlayer space of the C30B and have increased the distance between clay layers from 1.815 to 1.838 nm. A brief decrease in the interlayer

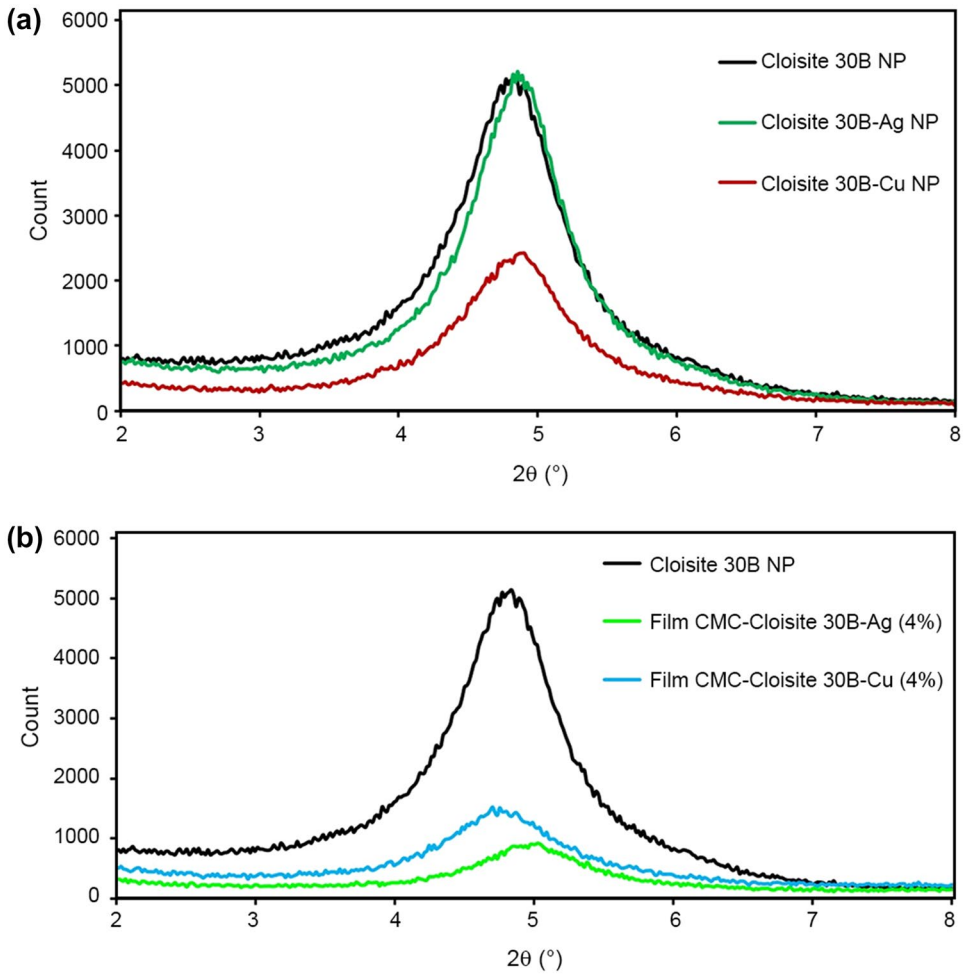

Fig. 2 XRD patterns of: **a** non-modified and Ag- or Cu-modified C30B; and **b** carboxymethyl cellulose films containing Ag- or Cu-modified C30B clay NPs

distance in the XRD pattern of the Cu-modified C30B is probably due to the exchange of Cu ions with ammonium cations of clay leading to inclusion of Cu ions into the clay layers. The results of the interlayer distance of these three types of clay are shown in Table 1. XRD patterns of the CMC-based nanocomposite films containing Ag- and Cu-modified C30B NPs are shown in Fig. 2b. Regarding the XRD pattern shown for CMC-based film containing Ag-modified C30B NPs and the appearance of the peak at 2θ of about 4°–5°, the existence of a laminar structure for these nanocomposites is well known. In the layered structure, the polymer matrix chains are interposed between the layers of the clay and increase the distance between the layers which lead to transfer of 2θ peak to low angles. The results of the interlayer distance of these nanocomposite films are reported in Table 1. As shown in Fig. 2b, a similar trend was observed for CMC-based nanocomposite films containing Cu-modified C30B NPs and the existence of a layered structure was characterized.

Scanning electron microscopy (SEM)

Figure 3 demonstrates SEM images of pure CMC film (a), CMC-based nanocomposite films containing 4 wt% of C30B-Ag (b), C30B-Cu (c), MMT-Ag (d), and MMT-Cu (e) clay NPs. As shown in Fig. 3a, the surface morphology of the pure CMC film was homogeneous indicating the crystalline structure of the biopolymer matrix. All nanocomposite films showed heterogeneous surface compared to pure CMC film which is likely related to aggregate NPs in the film matrix. By comparing all nanocomposite samples, it becomes clear that the film containing sodium montmorillonite (Na^+-MMT) clay NPs had more heterogeneous surface with more accumulated NPs compared to those of films incorporating C30B. This comparison shows that clay nanoparticles of C30B were more compatible with CMC matrix than MMT. Furthermore, films incorporating Cu-modified NPs had more homogeneous and uniform surface morphology than films containing Ag-modified NPs, indicating a better dispersion of Cu-modified NPs in the film matrix.

Table 1 Distance interval and 2θ angles of non-modified and modified C30B NPs and CMC-based nanocomposite films containing Ag- and Cu-modified clay NPs calculated by Bragg's law

NP/Nanocomposite films	2θ (°)	d_{001} (nm)
Cloisite 30B (C30B)	4.86	1.815
C30B-Cu	4.81	1.834
C30B-Ag	4.8	1.838
CMC-C30B (4 wt%)	4.31	2.046
CMC-C30B-Ag (4 wt%)	4.19	2.105
CMC-C30B-Cu (4 wt%)	4.39	2.009

Mechanical properties

The effect of the incorporation of various types of clays modified with Ag and Cu ions on the tensile strength (TS) and elongation-at-break (E) of pure CMC film and nanocomposite films containing various types of clay NPs is shown in Table 2. All nanocomposite films had significantly higher TS values than pure CMC film. This might be explained by the fact that the presence of clay NPs enhances interactions in CMC biopolymer matrix. Furthermore, nanocomposite films containing Ag- or Cu-modified C30B clay exhibited significantly higher TS values than those of the films containing different types of MMT. As already shown by SEM imagining (Fig. 3), clay NPs of C30B type were more compatible with CMC biopolymer matrix than MMT NPs. Organic modification of C30B clay increases their interaction with CMC matrix leading to more compatibility of these NPs with CMC bio-macromolecules. Among the analyzed film samples, the CMC-based film containing Cu-modified C30B and Ag-modified MMT NPs showed the highest and lowest TS values, respectively. Elongation-at-break was significantly ($P < 0.05$) higher for nanocomposite films than reference due to the presence of clay NPs (Table 2). Also, nanocomposite films containing C30B clay NPs (modified with Ag and Cu ions) showed higher E values than films containing all types of MMT clay.

UV–Visible spectroscopy of nanocomposite films

Figure 4 shows the effect of incorporating unmodified as well as Ag- or Cu-modified NPs of C30B (Fig. 4a) and MMT (Fig. 4b) clays on the UV absorbance of the resulting films at a wavelength range of 200–800 nm. There was no absorption peak in UV–Vis spectra of pure CMC film, indicating that it transmits UV radiation. Among the CMC-based films incorporating different types of C30B clay NPs, Ag-modified CMC-C30B film showed the UV absorption peak at a wavelength range of 390–480 nm. It is also clear from Fig. 4a that Cu-modified CMC-C30B film and CMC-film containing non-modified C30B NPs transmitted UV radiation and did not show any absorption. Figure 4b also demonstrates that CMC films containing Ag-modified MMT clay NPs showed the UV absorption peak in the wavelength range of 390–480 nm. Nanocomposite films containing non-modified as well as Cu-modified MMT NPs did not show any UV-absorption at a wavelength range of 390–480 nm.

Water vapor permeability of the films

One of the important requirements for the use of CMC biopolymer in food packaging is to reduce its WVP to the lowest possible level. Figure 5 shows WVP values of different films with/ without clay NPs incorporating different

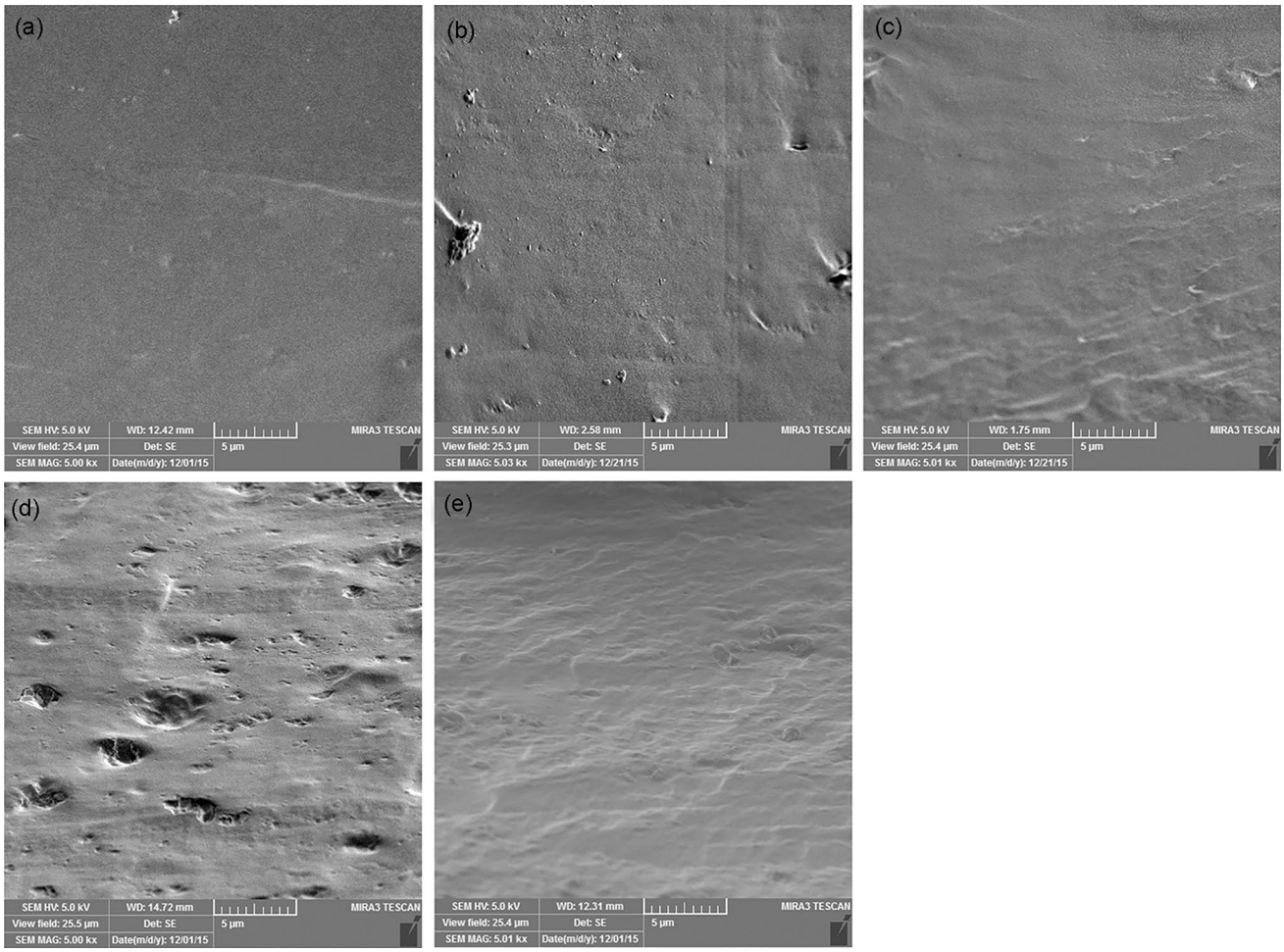

Fig. 3 SEM images of pure CMC film (**a**); CMC-based films containing 4 wt% of C30B-Ag (**b**), C30B-Cu (**c**), MMT-Ag (**d**), and MMT-Cu (**e**) clay NPs

Table 2 Variation of tensile strength (TS) and elongation-at-break (E) of pure CMC film and CMC-based nanocomposite films incorporating 4 wt% of different modified clay NPs

Nanocomposite films	TS (MPa)	*E* (%)
Pure CMC film	20.03 ± 1.52^{e}	30.35 ± 1.55^{d}
CMC-MMT-Ag	23.45 ± 1.40^{d}	34.67 ± 2.08^{c}
CMC-MMT-Cu	25.88 ± 0.87^{c}	37.55 ± 2.50^{c}
CMC-C30B-Ag	32.17 ± 1.05^{b}	52.12 ± 2.52^{b}
CMC-C30B-Cu	37.93 ± 1.15^{a}	58.63 ± 1.58^{a}

Data are mean of triplicate measurements ± SD. Different alphabetical letters in each column indicate significant ($P < 0.05$) differences between mean using Tukey's test

types of clay NPs. Incorporation of all types of clay NPs into the CMC biopolymer matrix significantly decreased WVP of nanocomposite films ($P < 0.05$). The effect of the presence of clay nanoparticles on reducing the WVP of nanocomposite films can be explained in various ways. The most important proposed mechanism is the presence of layers of clay NPs in the biopolymer matrix, which produces complex paths for the diffusion of vapor molecules [37]. In fact, in the presence of clay NPs, vapor molecules must pass a longer and more complex pathway which reduces the transfer and penetration of water vapor molecules [38]. As more nanoclay layers are distributed in the biopolymer matrix, the more these tortuous pathways are added, and the WVP of the film is decreased. This issue shows the importance of the type of dispersion of clay NPs in the film biopolymer matrix. Other proposed mechanisms include the filling of empty spaces, as well as the establishment of hydrogen bonds with CMC molecules, thereby reducing the diffusion of water molecules in the matrix [39]. Various researchers studied the relationship between the water vapor permeability of polymer matrix and the dispersion of clay NP layers and concluded that the greatest preventive factor against WVP is when the clay NPs are dispersed in the form of an exfoliated structure [38, 40]. Reduction in the WVP is related to strong

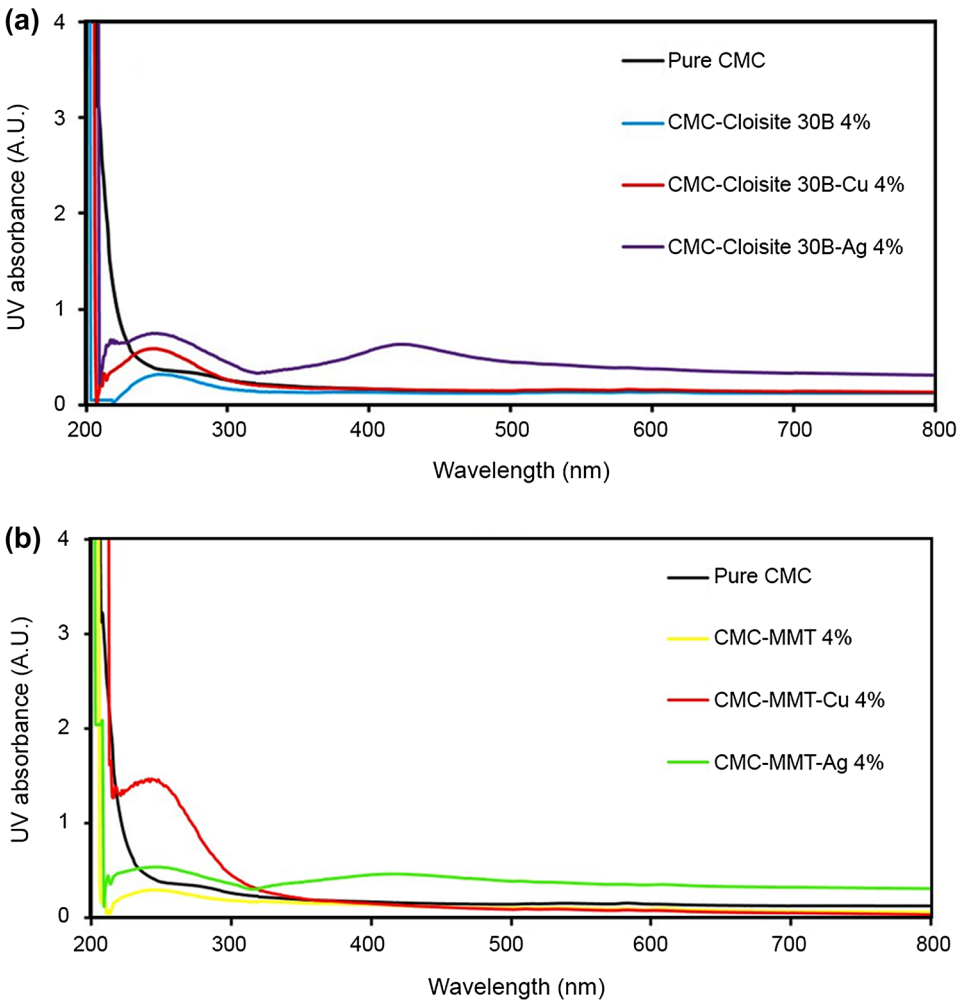

Fig. 4 The effect of incorporating unmodified as well as Ag- or Cu-modified NPs of C30B (**a**) and MMT (**b**) clay NPs on the UV absorbance of the resulting films in the wavelength range of 200–800 nm

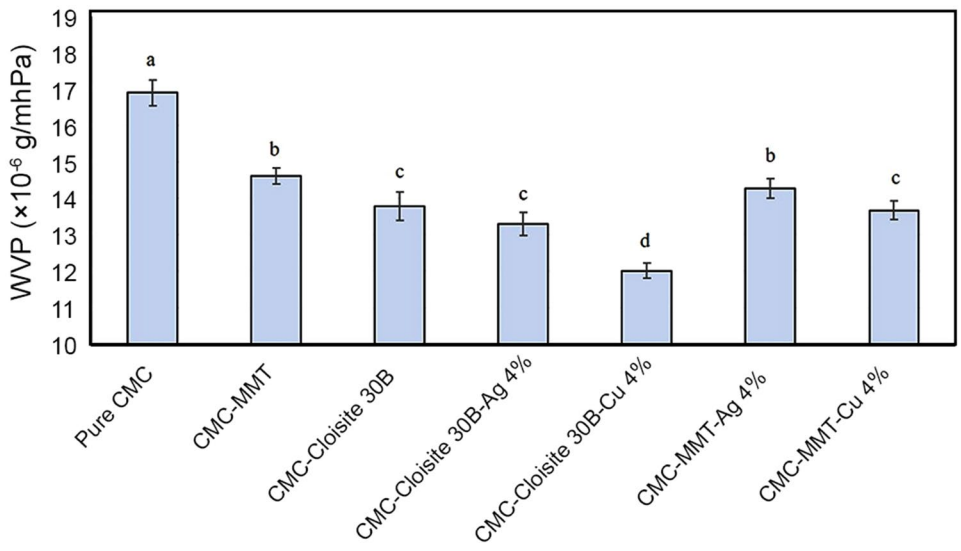

Fig. 5 WVP of pure CMC films and nanocomposite films incorporating different types of clay NPs

interaction between clay NPs and the biopolymer matrix, which affects the diffusion of permeates. In fact, these interactions affect the propagation parameter which determines the permeability level. The placement of layers of clay in the biopolymer chains reduces the free spaces and controls the emission rate of water molecules. Of course, in the case of a

Table 3 The diameter of the inhibition zone of pure CMC film and prepared nanocomposite films incorporating 4 wt% different types of clay NPs in the microbial test against *S. aureus* and *E. coli*

Nanocomposite films	Inhibition zone diameter (mm)	
	S. aureus	*E. coli*
Pure CMC film	0.00 ± 0.00^{g}	0.00 ± 0.00^{d}
CMC-C30B	4.90 ± 0.21^{d}	1.70 ± 0.15^{c}
CMC-C30B-Cu	5.72 ± 0.13^{c}	2.41 ± 0.12^{b}
CMC-C30B-Ag	9.87 ± 0.20^{a}	3.84 ± 0.11^{a}
CMC-MMT	0.87 ± 0.06^{f}	0.00 ± 0.00^{d}
CMC-MMT-Cu	2.45 ± 0.24^{e}	2.19 ± 0.23^{b}
CMC- MMT-Ag	6.66 ± 0.18^{b}	3.88 ± 0.19^{a}

Data are mean of duplicate measurements ± SD. Different alphabetical letters in columns indicate significant ($P < 0.05$) differences between means using Tukey's test

layered structure for nanocomposite films (according to the XRD analysis of prepared nanocomposite films in this study) deterrence is created against the passage of water vapor, but the amount of this permeability is low compared to the exfoliated structure. Finally, as shown in Fig. 5, the effect of the C30B-type clay NPs on WVP is greater than that of MMT-type. Moreover, reduction of the WVP of the films containing Cu-modified clay NPs was significantly ($P < 0.05$) higher than that of Ag-modified clay NPs of C30B. As shown by SEM imaging (Fig. 3), clay NPs of C30B type created more homogeneous surface morphology and was more compatible with CMC matrix compared to MMT NPs. This would result in filling the pathways inside the CMC biopolymer matrix leading to reduced WVP of the obtained films. Furthermore, films incorporating Cu-modified NPs had more homogeneous and uniform surface morphology than films containing Ag-modified NPs, indicating a better dispersion of Cu-modified NPs in the film matrix. This could explain the lower WVP of the films containing Cu-modified NPs.

Antibacterial properties

Table 3 shows inhibition zone diameters of pure CMC and nanocomposite films incorporating different types of clay NPs against *S. aureus* and *E. coli*. Pure CMC and CMC-MMT films with no metallic NPs showed no antibacterial effect (no inhibition zone). With the incorporation of C30B clay NPs into the CMC biopolymer matrix, the antimicrobial effect in films is observed with larger inhibition diameter, which means that the C30B clay NPs themselves have antibacterial effect. Nanocomposite films containing Ag-modified C30B clay NPs had higher antibacterial activity than Cu-modified type. It was also shown that antibacterial activities of CMC-C30B films modified with Ag and Cu metallic ions were higher than those of the corresponding CMC-MMT films. It was shown that Ag- or Cu-modified CMC-C30B films were more effective against *S. aureus* than *E. coli*. This shows that the gram-positive bacteria were more sensitive to effect of these nanoparticles than gram-negative bacteria.

Conclusion

CMC films incorporating different types of clay NPs, modified by Ag and Cu ions were prepared and their physico-mechanical and antibacterial properties were evaluated. XRD patterns for modified clays with Ag and Cu ions showed that they were effectively located in the interlayer space of C30B and MMT clay NPs and increased their interlayer spacing. A smooth and homogeneous structure for a pure CMC film was confirmed by SEM imaging. Incorporating clay NPs, turned homogeneous surface into a rough and more heterogeneous morphology. Moreover, film surface containing MMT clay NPs was coarser and more heterogeneous than that of C30B. Nanocomposite films exhibited higher TS values than pure CMC film due to the presence of clay NPs in the CMC biopolymer matrix. Nanocomposite films containing C30B clay NPs (modified with Ag and Cu ions) exhibited higher TS than those containing different types of MMT clay. This was due to the better compatibility of C30B clay NPs in the biopolymer matrix than MMT. UV–Visible analysis showed that CMC film containing 4 wt% Ag-modified C30B had higher UV absorption than other samples. With the incorporation of all types of clay NPs into the CMC matrix, WVP of nanocomposite films was significantly reduced. Pure CMC film and CMC-MMT films with no metallic NPs had no antibacterial effect against *S. aureus* and *E. coli*. With the incorporation of C30B clay NPs into the CMC biopolymer matrix, the antimicrobial effect in films is observed with increasing inhibition zone. Films containing Ag-modified C30B had higher antibacterial activity than Cu-modified type.

References

1. Fasihnia SH, Peighambardoust SH, Peighambardoust SJ, Oromiehie A (2018) Development of novel active polypropylene based packaging films containing different concentrations of sorbic acid. Food Packag Shelf Life 18:87–94
2. Wang W, Zhang H, Jia R, Dai Y, Dong H, Hou H, Guo Q (2018) High performance extrusion blown starch/polyvinyl alcohol/clay nanocomposite films. Food Hydrocoll 79:534–543
3. Han JW, Ruiz-Garcia L, Qian JP, Yang XT (2018) Food packaging: a comprehensive review and future trends. Compr Rev Food Sci Food Safe 17:860–877
4. Reddy MM, Vivekanandhan S, Misra M, Bhatia SK, Mohanty AK (2013) Biobased plastics and bionanocomposites: current status and future opportunities. Prog Polym Sci 38:1653–1689

5. Rachtanapun P, Luangkamin S, Tanprasert K, Suriyatem R (2012) Carboxymethyl cellulose film from durian rind. LWT Food Sci Tech 48:52–58
6. Toğrul H, Arslan N (2004) Carboxymethyl cellulose from sugar beet pulp cellulose as a hydrophilic polymer in coating of mandarin. J Food Eng 62:271–279
7. Espitia PJP, Soares NdFF, Teófilo RF, dos Reis Coimbra JS, Vitor DM, Batista RA, Ferreira SO, de Andrade NJ, Medeiros EAA (2013) Physical–mechanical and antimicrobial properties of nanocomposite films with pediocin and ZnO nanoparticles. Carbohydr Polym 94:199–208
8. Oun AA, Rhim J-W (2017) Preparation of multifunctional chitin nanowhiskers/ZnO-Ag NPs and their effect on the properties of carboxymethyl cellulose-based nanocomposite film. Carbohydr Polym 169:467–479
9. Paul M-A, Delcourt C, Alexandre M, Degée P, Monteverde F, Dubois P (2005) Polylactide/montmorillonite nanocomposites: study of the hydrolytic degradation. Polym Degrad Stab 87:535–542
10. Rhim J, Wang L, Hong S (2013) Preparation and characterization of agar/silver nanoparticles composite films with antimicrobial activity. Food Hydrocoll 33:327–335
11. El Sayed A, El-Gamal S (2015) Synthesis and investigation of the electrical and dielectric properties of Co_3O_4/(CMC+ PVA) nanocomposite films. J Polym Res 22:1–12
12. Thostenson ET, Li C, Chou T-W (2005) Nanocomposites in context. Compos Sci Technol 65:491–516
13. Dehghani S, Peighambardoust SH, Peighambardoust SJ, Hosseini SV, Regenstein JM (2019) Improved mechanical and antibacterial properties of active LDPE films prepared with combination of Ag, ZnO and CuO nanoparticles. Food Packag Shelf Life 22:100391
14. Fasihnia SH, Peighambardoust SH, Peighambardoust SJ (2018) Nanocomposite films containing organoclay nanoparticles as an antimicrobial (active) packaging for potential food application. J Food Proc Preserv 42:e13488
15. Li X, Xing Y, Jiang Y, Ding Y, Li W (2009) Antimicrobial activities of ZnO powder-coated PVC film to inactivate food pathogens. Int J Food Sci Tech 44:2161–2168
16. Peighambardoust SJ, Peighambardoust SH, Pournasir N, Mohammadzadeh-Pakdel P (2019) Properties of active starch-based films incorporating a combination of Ag, ZnO and CuO nanoparticles for potential use in food packaging applications. Food Packag Shelf Life 22:100420
17. Wojcieszak D, Kaczmarek D, Antosiak A, Mazur M, Rybak Z, Rusak A, Osekowska M, Poniedzialek A, Gamian A, Szponar B (2015) Influence of Cu–Ti thin film surface properties on antimicrobial activity and viability of living cells. Mater Sci Eng C 56:48–56
18. Zapata PA, Tamayo L, Páez M, Cerda E, Azócar I, Rabagliati FM (2011) Nanocomposites based on polyethylene and nanosilver particles produced by metallocenic "in situ" polymerization: synthesis, characterization, and antimicrobial behavior. Eur Polym J 47:1541–1549
19. Ebrahimi Y, Peighambardoust SJ, Peighambardoust SH, Zahed-Karkaj S (2019) Development of antibacterial carboxymethyl cellulose-based nanobiocomposite films containing various metallic nanoparticles for food packaging applications. J Food Sci 84:2537–2548
20. Peighambardoust SH, Beigmohammadi F, Peighambardoust SJ (2016) Application of organoclay nanoparticle in low-density polyethylene films for packaging of UF cheese. Packag Technol Sci 29:355–363
21. Su PG, Huang LN (2007) Humidity sensors based on TiO_2 nanoparticles/polypyrrole composite thin films. Sens Actuat B 123:501–507
22. Youssef AM, El-Sayed SM (2018) Bionanocomposites materials for food packaging applications: concepts and future outlook. Carbohydr Polym 193:19–27
23. Zafar R, Mahmood Zia K, Tabasum S, Jabeen F, Noreen A, Zuber M (2016) Polysaccharide based bionanocomposites, properties and applications: a review. Int J Biol Macromol 92:1012–1024
24. Magana S, Quintana P, Aguilar D, Toledo J, Angeles-Chavez C, Cortes M, Leon L, Freile-Pelegrín Y, Lopez T, Sánchez RT (2008) Antibacterial activity of montmorillonites modified with silver. J Mol Catal A 281:192–199
25. Kim YH, Lee DK, Cha HG, Kim CW, Kang YS (2007) Synthesis and characterization of antibacterial Ag− SiO_2 nanocomposite. J Phys Chem C 111:3629–3635
26. Nottagh S, Hesari J, Peighambardoust SH, Rezaei-Mokarram R, Jafarizadeh-Malmiri H (2018) Development of a biodegradable coating formulation based on the biological characteristics of the Iranian ultra-filtrated cheese. Biologia 73:403–413
27. Nottagh S, Hesari J, Peighambardoust SH, Rezaei-Mokarram R, Jafarizadeh-Malmiri H (2020) Effectiveness of edible coating based on chitosan and Natamycin on biological, physicochemical and organoleptic attributes of Iranian ultra-filtrated cheese. Biologia 75:605–611
28. Aghamirzaei M, Peighambardoust SH, Azadmard-Damirchi S, Majzoobi M (2015) Effects of grape seed powder as a functional ingredient on flour physicochemical characteristics and dough rheological properties. J Agric Sci Technol 17:365–373
29. Bhunia K, Sablani SS, Tang J, Rasco B (2013) Migration of chemical compounds from packaging polymers during microwave, conventional heat treatment, and storage. Compr Rev Food Sci Food Safe 12:523–545
30. Hajizadeh H, Peighambardoust SJ, Peighambardoust SH, Peressini D (2020) Physical, mechanical, and antibacterial characteristics of bio-nanocomposite films loaded with Ag-modified SiO_2 and TiO_2 nanoparticles. J Food Sci 85:1193–1202
31. Zienkiewicz-Strzałka M, Deryło-Marczewska A, Kozakevych R (2018) Silica nanocomposites based on silver nanoparticles-functionalization and pH effect. Appl Nanosci 8:1649–1668
32. Khodaeimehr R, Peighambardoust SJ, Peighambardoust SH (2018) Preparation and characterization of corn starch/clay nanocomposite films: effect of clay content and surface modification. Starch-Stärke 70:1700251
33. Singh S, Lee MH, Park I, Shin YJ, Lee YS (2016) Antimicrobial properties of polypropylene films containing $AgSiO_2$, AgZn and AgZ for returnable packaging in seafood distribution. J Food Measur Charact 10:781–793
34. Beigmohammadi F, Peighambardoust SH, Hesari J, Azadmard-Damirchi S, Peighambardoust SJ, Khosrowshahi NK (2016) Antibacterial properties of LDPE nanocomposite films in packaging of UF cheese. LWT Food Sci Tech 65:106–111
35. Durmuş A, Woo M, Kaşgöz A, Macosko CW, Tsapatsis M (2007) Intercalated linear low density polyethylene (LLDPE)/clay nanocomposites prepared with oxidized polyethylene as a new type compatibilizer: structural, mechanical and barrier properties. Eur Polym J 43:3737–3749
36. González Sandoval DC, Luna Sosa B, Martínez-Ávila GCG, Rodríguez Fuentes H, Avendaño Abarca VH, Rojas R (2019) Formulation and characterization of edible films based on organic mucilage from Mexican *Opuntia ficus-indica*. Coatings 9:506
37. Shahabi-Ghahfarrokhi I, Babaei-Ghazvini A (2019) Using photo-modification to compatibilize nano-ZnO in development

of starch-kefiran-ZnO green nanocomposite as food packaging material. Int J Biol Macromol 124:922–930
38. Kanmani P, Rhim J-W (2014) Physical, mechanical and antimicrobial properties of gelatin based active nanocomposite films containing AgNPs and nanoclay. Food Hydrocoll 35:644–652
39. Ma X, Chang PR, Yang J, Yu J (2009) Preparation and properties of glycerol plasticized-pea starch/zinc oxide-starch bionanocomposites. Carbohydr Polym 75:472–478
40. Bajpai S, Chand N, Chaurasia V (2010) Investigation of water vapor permeability and antimicrobial property of zinc oxide nanoparticles-loaded chitosan-based edible film. J Appl Polym Sci 115:674–683